IET Electric Power Applications

Research Article

IET Journals
The Institution of Engineering and Technology

Characteristic analysis and design of novel high-frequency shell-type coaxial transformer

ISSN 1751-8660
Received on 12th November 2018
Revised 9th July 2019
Accepted on 22nd July 2019
E-First on 1st October 2019
doi: 10.1049/iet-epa.2018.5815
www.ietdl.org

Yoon-Sun Lee[1], Kyoung-Tak Kim[2], Joung-Hu Park[2], Seung-Jae Lee[3], Tae-Kyung Chung[4], Jong-Suk Ro[4] ✉

[1]*Electrotechnology R&D Division, LSIS Co., Ltd, Cheongju, Republic of Korea*
[2]*Department of Electrical Engineering, Soongsil University, Dongjak-gu, Seoul, Republic of Korea*
[3]*Department of Electrical and Computer Engineering, Seoul National University, Gwanak-gu, Seoul, Republic of Korea*
[4]*Department of Electrical and Electronics Engineering, Chung-Ang University, Dongjak-gu, Seoul, Republic of Korea*
✉ *E-mail: jongsukro@gmail.com*

Abstract: Recently, power conversion systems (PCSs) have exhibited high efficiencies and miniaturisation, and this trend is expected to grow in the future. An important component of the PCS, which accounts for a significant portion of its volume, is the transformer (TR). However, it is difficult to achieve a significant increase in the efficiency and reduction in the volume of a PCS using a conventional TR, as the conventional TRs do not offer much scope for further optimisation. To overcome this limitation imposed by the conventional TRs, a novel and practical high-frequency coaxial TR, named the shell-type coaxial TR (SCTR), is proposed in this work. A useful and strategic analysis and design method, which covers the overall development process from the design stage to the experimental validation stage of the proposed high-frequency SCTR, is also proposed. The usefulness of the proposed SCTR and the analysis and design method are verified by designing an SCTR for a 50 W DC/DC converter and conducting experiments on it. It is found that the use of the proposed technique can cause a significant increase in the efficiency and power density of the PCS

1 Introduction

Recently, electric power systems have exhibited a trend of high efficiency and high power density. This has led the way to research on the reduction of power losses and increase of efficiency of electric power conversion systems (PCSs) of the electric power systems [1–3]. Among the many components of PCSs, magnetic devices such as transformers (TRs) account for a considerable portion of the cost, size, and efficiency. For example, DC/DC switching converters are one of the major categories of PCSs. The TR is a significant component of the converter, which determines its size and efficiency [4–6].

By increasing the magnetic flux density and reducing the leakage inductance of the TR, efficiency improvement and volume reduction can be achieved. However, the conventional TR has been optimised almost fully [7–12]. Hence, it will be difficult to improve the efficiency or reduce the volume of a conventional TR, significantly, which in turn makes it difficult to optimise a converter using the conventional TR. Therefore, an innovative and novel TR is necessary to improve the efficiency and power density of TRs and PCSs.

To address these problems, a novel and practical coaxial TR, termed the shell-type coaxial TR (SCTR), is proposed in this work. In the proposed SCTR, the primary winding (PW) and secondary winding (SW) are coaxial, unlike the conventional TR, which can help reduce the leakage flux and improve efficiency. As the PW and SW share an axis, the magnetic coupling is significantly high, with a high coupling coefficient, similar to that of an ideal TR. Moreover, the shell-type core of the SCTR improves practicality and compatibility. By applying the proposed novel and practical SCTR in a converter, the efficiency and power density of the converter can be increased dramatically [13–18].

While there have been many reports on the characteristic analysis and design methods for conventional TRs [4, 19–22], an analysis and design method for the SCTR has not been proposed yet. This paper presents a rapid and accurate analysis method and a strategic design technique for SCTRs.

Specifically, we propose a useful characteristic analysis method that uses an equivalent circuit model, an analytic method, a finite element method (FEM), and an experiment, for SCTR. Moreover, a strategic and specific design method, which covers the entire development process of the SCTR, from design to experiment, is also proposed. The usefulness of the proposed SCTR, characteristic analysis method, and design method are confirmed via the design, manufacturing, and experimental analysis of an SCTR applied to a 50 W step-down flyback converter. The flyback converter is chosen, as it is one of the most preferred DC/DC converters for this range of power, owing to its simple structure and reliable insulation.

2 Structure and working principle of SCTR

The value of the coupling coefficient reflects the leakage between the PW and SW. The coupling coefficient value is mainly determined by the distance between the PW and SW. Therefore, to mitigate the leakage between the PW and SW, diverse approaches such as sandwich winding have been used.

However, the winding methods for conventional TRs have limitations in reducing the distance between the PW and SW. Hence, the coupling coefficient cannot be increased significantly, when using a conventional TR. To increase the value of the coupling coefficient dramatically, an SCTR in which the axes of the PW and SW are in a line is proposed in this paper. The proposed SCTR is advantageous in terms of manufacturing and commercialisation, as it uses a standardised shell-type core, as shown in Fig. 1. The inner winding is composed of conductors connected in series and is considered to be the PW. The outer winding is a tube-shaped conductor covering the inner winding and is considered to be the SW. The inner and outer windings are wound around the shell-type core.

Owing to the geometric uniqueness of the windings of the SCTR, the magnetic flux leakage between the PW and SW is less. Hence, the efficiency of both the TR and PCS can be improved significantly by applying the SCTR.

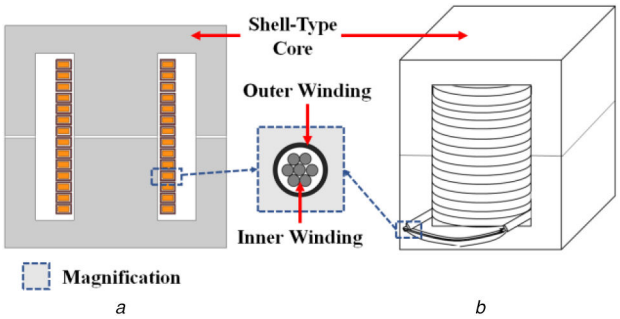

Fig. 1 *Proposed SCTR*
(a) 2D cross-sectional view, ***(b)*** 3D view

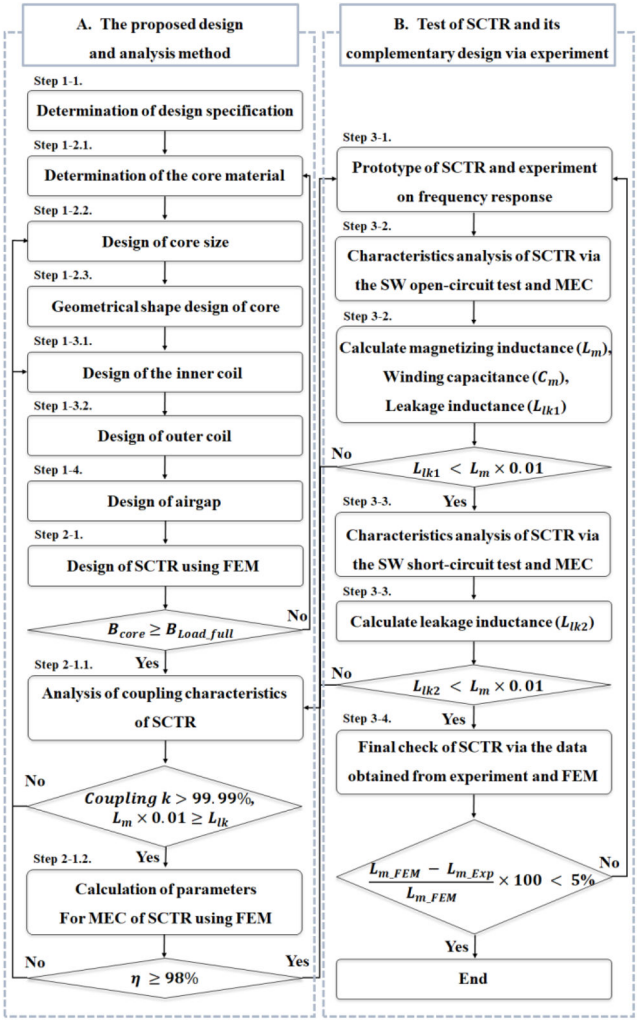

Fig. 2 *Proposed design flow chart for SCTR*

3 Proposed analysis and design method for SCTR

In this section, the important design variables and the characteristic analysis method for SCTR are discussed. A strategic design method based on the proposed flow chart demonstrated in Fig. 2 is also explained.

3.1 Proposed design method of the SCTR by using analytic method

3.1.1 Determination of design specifications: In the high-frequency operation of the TR, the inductance effect is dominant. Similarly, the effect of the leakage inductance is increased as the operating frequency is increased. The non-desirable effects of the leakage inductance include: increase in the magnetic loss, voltage drop, switching voltage, etc. Hence, the leakage inductance has significant effects on the efficiency and power density of the high-frequency TR. In other words, the reduction of the leakage inductance can improve the efficiency and power density of the TR.

In this paper, an SCTR with significantly low leakage inductance is proposed, which will be useful for high-frequency operations. The efficiency and power density of the PCS used in high-frequency applications such as in power converters can be increased dramatically via the application of the SCTR.

For verifying the usefulness of the proposed SCTR in high-frequency applications, it is applied in a flyback power converter operating at 50 W. The design constraints of the SCTR, based on the specifications of the flyback converter, are tabulated in Table 1.

Table 1 Design constrains of SCTR based on the specifications of a flyback converter

Symbol	Parameter	Spec.
V_{in}	input voltage of the converter	100 V_{dc}
V_{out}	output voltage of converter	50 V_{dc}
P_{out}	output power of the converter	50 W
f_s	switching frequency	30 kHz
N	SCTR turns ratio	1:2

3.1.2 Design of core: The iron loss of the TR is composed of the eddy-current loss and hysteresis loss. The eddy current loss and hysteresis loss are increased as the operation frequency is raised depending on magnetic material characteristics [23, 24]. Hence, the iron loss is an important factor to be considered in the design of high-frequency SCTR.

The application of SCTR in this research is 30 kHz, the high-operating frequency. Hence, the iron loss of SCTR can be huge and the design of SCTR to reduce the iron loss is important.

The mitigation of iron loss is possible by the proper choice of material, size, and shape of core in the design stage.

Determination of the core material: In the design of core, performance, cost, commercialisation, and others must be considered in a comprehensive manner. Therefore, Mn-Zn ferrite material core is selected for high frequency operating SCTR in this study. Mn-Zn ferrite material core is standardised with low cost and can operate from 1 kHz–1 MHz [25–27]. Moreover, because of the high permeability of Mn-Zn ferrite, it is possible to design a TR with a low number of coil turns for high output power. A low number of coil turns can minimise the copper loss of coil due to joule effect, which explains that it can reduce the heat generation that causes copper loss.

Design of core size: After the core material of the TR is determined, the size of the core must be designed considering the operating frequency and output power. By determining the core size properly, the flux saturation and loss can be reduced.

The total size of the core can be determined from the area ratio A_p, which is the product of the cross-sectional area A_c of the core and the cross-sectional area W_a of the winding, as derived in (1), where P_0 is the output power, K is a constant related to the switching frequency, and f is the switching operating frequency. $\triangle B$ is the difference between the maximum magnetic flux density and the available maximum magnetic flux density. The effective permeability decreases due to the switching and temperature rise of the DC/DC converter. Therefore, the difference caused by this reduction is defined as $\triangle B$. Considering the specifications of the TR and the material properties of Manganese-Zinc Ferrites used in this paper, the effective permeability reduction rate is about 1.67%. Thus, when the maximum magnetic flux density is 0.3 T, $\triangle B$ is derived as 0.0049 T [28]. Applying the material properties and output power into (1), the area ratio A_p for the 50 W SCTR is calculated as 9.45 cm^2.

$$A_p = W_a A_c = \left(\frac{P_0}{K \times \Delta B \times f}\right)^{4/3} \quad (1)$$

IET Electr. Power Appl., 2019, Vol. 13 Iss. 12, pp. 2027-2034

Design geometrical shape of core: In Step 1–2.1, Mn-Zn ferrite was selected as a suitable core material for high-frequency applications, considering its efficiency and cost.

In this research, commercially available ferrite core was used, considering compatibility and cost. There are several types of commercially available ferrite cores manufactured according to the IEC standard. Considering the application, size, cost, etc., the PQ40/40 ferrite core (TDK Co.) equipped with a bobbin is chosen as the core of the SCTR applied in the step-down flyback converter.

3.1.3 Design of winding: When a coaxial cable is connected to a high-frequency SCTR, a current with the frequency higher than that of the current flowing through a typical cable flows through the SCTR. A high-frequency current flows in both the inner and outer coil windings of the high-frequency SCTR. Moreover, the distance between the inner and outer coils is too small. Hence, the skin effect and proximity effect must be considered in the design stage.

As the PW and SW are extremely close, unlike in conventional TRs, the parasitic capacitance of the proposed SCTR cannot be ignored and should be checked in the winding design stage.

The number of turns N_p can be designed using (2), where N_p is the number of turns of the PW, V_p is the input voltage of the SCTR, K_f is a form factor for square-wave excitation, B_m is the maximum magnetic flux density, A_c is the cross-sectional area of the core, and f is the operating frequency.

The number of turns for the PW and SW are 14 and 28, respectively, according to the turns ratio.

$$N_p = \frac{V_p \times 10^4}{K_f \times B_m \times f \times A_c} \tag{2}$$

Design of the inner coil: To mitigate the skin effect arising from the high-frequency current flowing in the inner and outer coils of the SCTR, and the proximity effect arising from the inner and outer coils being extremely close, a Litz-type wire is adopted for the inner-coil winding (PW), of the SCTR, in this research.

The skin effect refers to the phenomenon which the AC current density decreases as it gets closer to the centre of the conductor. In order to reduce the skin effect, Litz Wire can be effectively used to transmit and control the amount of the current. A Litz-type wire coil is a braided shape formed by bundling a plurality of coils with small cross-sections into one bundle, as shown in Fig. 1. An enamel copper wire with a cross-sectional area of 2 mm^2 is used for the inner strand, in this research [29, 30].

Design of the outer coil: The commonly used enamelled copper cannot be used in the outer coil because the outer coil must be of a tubular shape, to surround the inner coil. Therefore, a disordering wire with >95% copper is used for the outer coil, taking into consideration the factors such as conduction, cost, mass production, etc.

For the optimal design of the TR, the cooper loss should be taken into consideration for designing the winding. The diameter of the winding that can optimise the cooper loss is determined Bessel function.

Based on the Maxwell equations, the analytical expression to evaluate the AC resistance factor (F_R) of multilayer winding was derived by Dowell by (3).

$$F_R = \frac{\triangle}{2\sqrt{2}}\left[R_S(\triangle) - 2\pi\eta^2\left(\frac{4(m^2-1)}{3}+1\right)R_P(\triangle)\right] \tag{3}$$

Where $\triangle$ is the normalised foil thickness with respect to the skin depth δ, m is the number of winding layers for a winding portion and η is the porosity factor. In the equation, $R_S(\triangle)$ and $R_P(\triangle)$ are specifically defined as below equations by (4), (5).

$$R_S(\triangle) = \frac{\mathrm{ber}\left(\frac{\triangle}{\sqrt{2}}\right)\mathrm{bei}'\left(\frac{\triangle}{\sqrt{2}}\right) - \mathrm{bei}\left(\frac{\triangle}{\sqrt{2}}\right)\mathrm{ber}'\left(\frac{\triangle}{\sqrt{2}}\right)}{\left[\mathrm{ber}'\left(\frac{\triangle}{\sqrt{2}}\right)\right]^2 + \left[\mathrm{bei}'\left(\frac{\triangle}{\sqrt{2}}\right)\right]^2} \tag{4}$$

$$R_P(\triangle) = \frac{\mathrm{ber}_2\left(\frac{\triangle}{\sqrt{2}}\right)\mathrm{ber}'\left(\frac{\triangle}{\sqrt{2}}\right) + \mathrm{bei}_2\left(\frac{\triangle}{\sqrt{2}}\right)\mathrm{bei}'\left(\frac{\triangle}{\sqrt{2}}\right)}{\left[\mathrm{ber}\left(\frac{\triangle}{\sqrt{2}}\right)\right]^2 + \left[\mathrm{bei}\left(\frac{\triangle}{\sqrt{2}}\right)\right]^2} \tag{5}$$

Here, ber and bei are Kelvin functions, where each respectively represents the real and imaginary parts of Bessel functions of the first kind. The cross-sectional area of the outer coil can be calculated using the Bessel differential function as 3.36 mm^2 [31, 32]. The cross-sectional area of the outer coil is confirmed by checking the leakage inductance, in Step 2.1.

3.1.4 Design of airgap: When the SCTR is operated at high frequencies, the inductance component becomes dominant, in accordance with (6), and the reactance of magnetisation inductance becomes large. Hence, the SCTR operating at a high frequency requires much current and energy for magnetisation. The SCTR stores energy in the form of a magnetic field in the core. Hence, the airgap is used by the SCTR to store large amounts of energy [33].

$$Z = R + \mathrm{j}\omega L \tag{6}$$

The length of the air gap χ_{airgap} for SCTR is generally 0 mm < χ_{airgap} < 1 mm, and it can be calculated using (7), where R_f is the magnetoresistance of the iron core, μ_r is the relative permeability of the iron core, μ_0 is the permeability of air, and A is the cross-sectional area of the core. The air gap of SCTR is determined from (7) as 0.5 mm, in this research.

$$x = \frac{N^4\mu_r\mu_0 l(A - N^2/R_f)}{R_f(1-\mu_r)} \tag{7}$$

3.2 Proposed analysis method of the SCTR using Magnetic Equivalent Circuit (MEC) and FEM

3.2.1 Design of SCTR using FEM: In this step, the initial design result is revised and verified through FEM. The usefulness of the proposed SCTR can also be confirmed in the design stage using FEM [34–38].

The characteristics of the electric equipment are closely related to the magnetic field distribution in the equipment. In order to calculate the self-equivalent circuit constants of the high-frequency coaxial TR that required in the paper, the magnetic field distribution analysis of the TR is essential. The distribution of the magnetic field depends on the structure of the TR and the magnetic properties of the material and the Maxwell equation is used as the governing equation to analyse it

$$\nabla^2 \boldsymbol{A} = -\mu \boldsymbol{J} \tag{8}$$

$$\boldsymbol{A} = 0 \tag{9}$$

In the above equation, $\boldsymbol{A}$ is the vector potential, μ is the iron core permeability, and $\boldsymbol{J}$ is the current density. As a result of the calculation using the Maxwell equation, the magnetic flux density $\boldsymbol{B}$ can be expressed as (10) using the vector potential $\boldsymbol{A}$.

$$\boldsymbol{B} = \nabla \times \boldsymbol{A} \tag{10}$$

The flux(Φ) in the iron core is expressed by (11) and the inductance L by (12). In this equation, S is the cross-sectional area in the core and N is the number of turns.

$$\Phi = \int \boldsymbol{B} \cdot \mathrm{d}s \tag{11}$$

$$L = \frac{N\Phi}{I} \tag{12}$$

In this study, a commercial tool Ansys is used for FEM. Owing to the geometry of SCTR, which does not vary in terms of depth, two-dimensional (2D) FEM is used in this study.

The detailed design and design modifications are conducted in this step through the FEM of the characteristics such as magnetic flux density, voltage ratio, iron loss, copper loss, etc.

To check and modify the initial design results of the shape, size, and material of the SCTR, the magnetic saturation level must be checked in this step. Fig. 3 shows the magnetic flux density distribution of the SCTR, at the full-load condition of 50 VA, to check the degree of magnetic saturation. From Fig. 3, it is confirmed that design of the core is appropriate, in terms of the size and material.

Moreover, the main performances such as conversion ratio and efficiency of the SCTR are checked in this step. From the data shown in Fig. 4, it is confirmed that the primary voltage (PV) and secondary voltage are converted in the ratio 2:1 and the efficiency is 98.65%, which satisfies the design requirements.

The detailed design results of the SCTR derived through the proposed design method and FEM via Step 1.1–1.4 are tabulated in Table 2.

The obtained specifications of the SCTR are used for the calculation of parameters for creating the MEC of the SCTR, in the next step.

Analysis of coupling characteristics of SCTR: The proposed SCTR can be modified for various power levels or types. Therefore, the following coupling-characteristic analysis method is proposed to estimate and check the coupling coefficients of the various types of SCTRs.

The leakage of magnetic flux in the SCTR is very small because the SW structurally covers the PW. Hence, the SCTR has a high coupling coefficient, almost similar to that of an ideal TR. The coupling between the PW and SW can be expressed by the MEC, in diverse forms, as shown in Fig. 5, and the coupling coefficient can be calculated using (13), where k_{12} is the coupling coefficient between the PW and SW, L_p is the primary magnetic inductance, L_s is the secondary magnetic inductance, L_M is the mutual inductance between the PW and SW, L_{ser} is the inductance of the PW and SW connected in series as shown in Fig. 5*b*, and L_{par} is the inductance of the PW and SW connected in parallel as shown in Fig. 5*c*

$$k_{12} = \frac{L_M}{\sqrt{L_p L_s}} = \frac{L_{ser} - L_{par}}{4\sqrt{L_p L_s}} \tag{13}$$

The measured coupling-coefficient value shown in Table 3 confirms that the proposed and designed SCTR satisfies the high coupling-coefficient requirement.

Calculation of parameters for MEC of SCTR using FEM: A TR can be expressed by a MEC composed of two or more electrical circuits and a magnetically coupled magnetic circuit [39–43]. The MEC of an SCTR can be expressed as in Fig. 6, where R_p is the PW resistance, L_{lk1} is the PW leakage inductance, L_m is the magnetising inductance, C_m is the parasitic capacitance between the PW and SW, R_s is the SW resistance, and L_{lk2} is the SW leakage inductance.

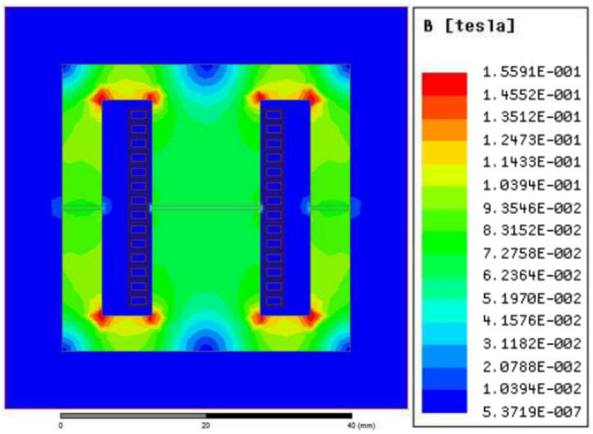

Fig. 3 *Magnetic flux density distribution of the SCTR in the full-load condition*

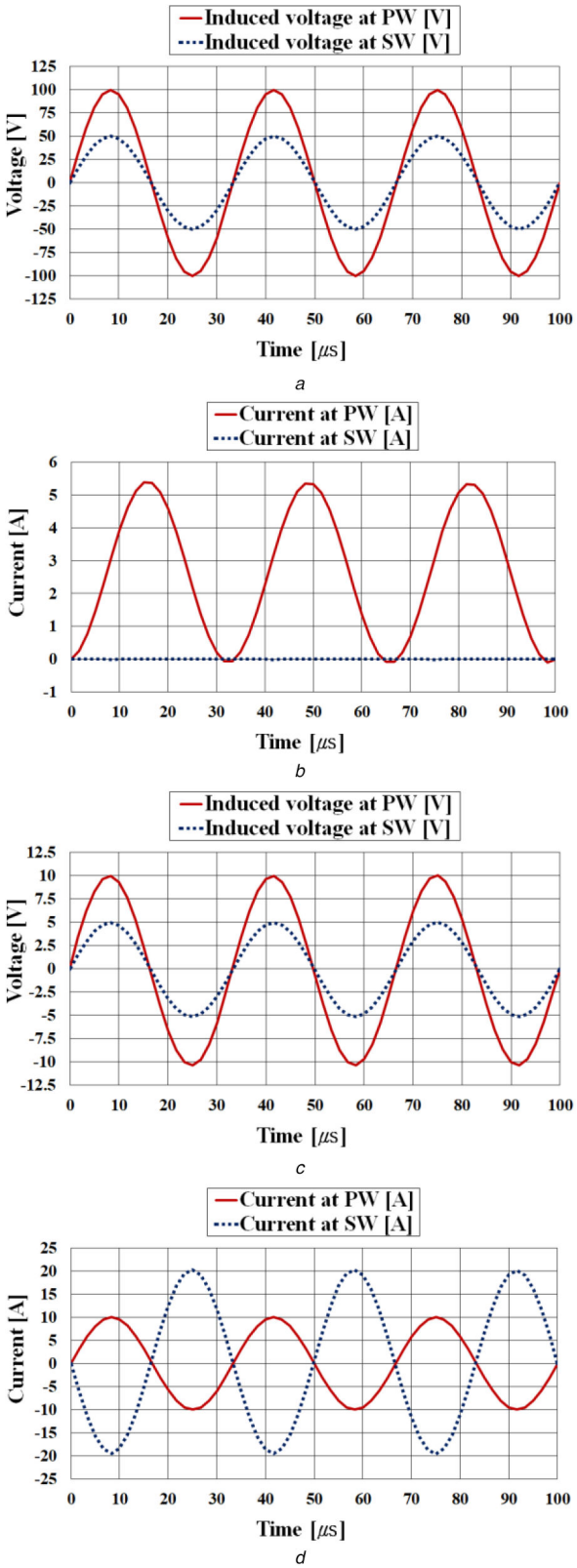

Fig. 4 *FEM results of SCTR*

(a) Induced voltages of PW and SW in the no-load condition, ***(b)*** Currents in the PW and SW in no-load condition, ***(c)*** Induced voltages of PW and SW in full-load condition, ***(d)*** Currents in the PW and SW in full-load condition

Table 2 Detailed design results of SCTR derived using the proposed design method and FEM via Steps 1.1–1.4

Design variable			Unit	Value
core	material		—	Mn-Zn ferrite
	length × width × height		mm	40 × 40 × 40
	window area		mm^2	210
coil	cross-section	primary coil	mm^2	2
		secondary coil		3.36
	resistance	primary coil	Ω	0.05
		secondary coil		0.025
airgap	length		mm	0.5

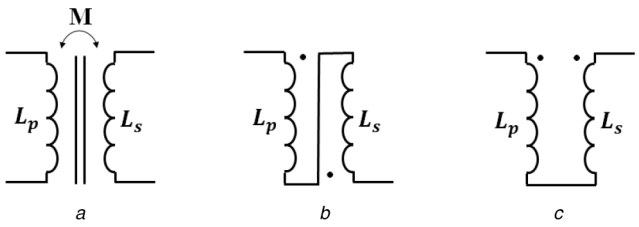

Fig. 5 *MECs for PW and SW of SCTR expressed by*
(a) Magnetic inductances L_P and L_S and mutual inductance L_m, ***(b)*** Inductances connected in series, ***(c)*** Inductances connected in parallel

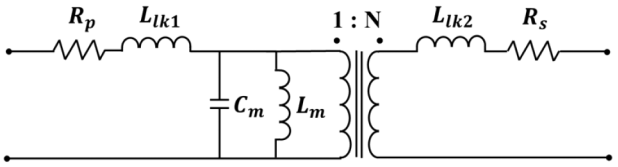

Fig. 6 *MEC of SCTR*

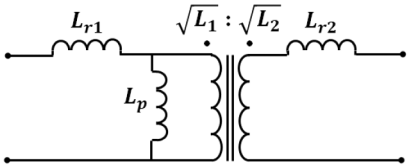

Fig. 7 *MEC for SCTR expressed by the obtainable parameters through FEM and (6)–(8)*

The parameters of the MEC shown in Fig. 6 are useful for analysing the characteristics of the TR, such as the efficiency, leakage, etc., and can be obtained through the open-circuit and short-circuit tests as shown in Section B.

Another expression of the MEC for SCTR is shown in Fig. 7, where L_{r1} is the magnetic inductance of the PW, L_{r2} is the magnetic inductance of the SW, and L_p is the mutual inductance. All parameters in Fig. 7 can be calculated by FEM and by using (14)–(16). The magnetic inductances of the PW L_1 and SW L_2 obtained using FEM are shown in Table 4. The coupling coefficient k is calculated from (13) as 0.9999. Finally, the parameters in Fig. 7 calculated using FEM and (14)–(16) are shown in Table 5.

$$L_{r1} = (1 - k)L_1 \tag{14}$$

$$L_s = kL_2 \tag{15}$$

$$L_p = kL_1 \tag{16}$$

3.3 Test of SCTR and Its complementary design via experiment

3.3.1 Prototype of SCTR and experiment on frequency response: The prototype of the SCTR designed by the proposed analysis and design method is shown in Fig. 8. An useful way to measure MEC parameters experimentally is by measuring the impedance of the PW over a wide frequency range when the SW is

Table 3 Data of inductances and coupling factors of SCTR obtained via experiments and analysis

Symbol	Parameter	Spec.
L_p	PW magnetic inductance	147 μH
L_s	SW magnetic inductance	630 μH
L_{ser}	inductance of PW and SW connected in series	1400 μH
L_{pal}	inductance of PW and SW connected in parallel	17 μH
K_{12}	coupling coefficient between PW and SW	99.99%

Table 4 Magnetic inductance obtained through FEM

Parameter	L_1	L_2
values calculated by FEM	197.15 μH	98.46 μH

Table 5 Calculated parameters of Fig. 8 for SCTR

Parameter	L_P	L_{r1}	L_{r2}
calculated results, μH	197.06	0.10	0.023

Fig. 8 *Prototype of SCTR designed by the proposed analysis and design method*

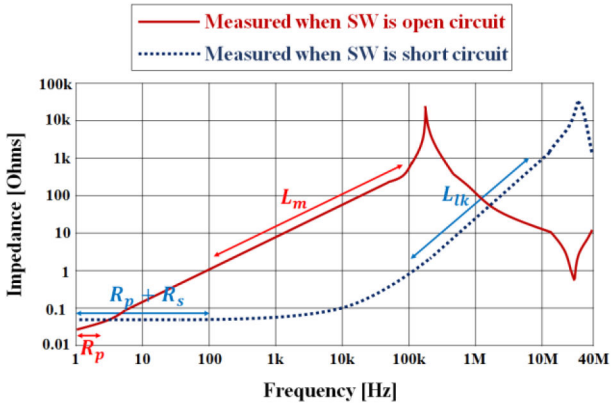

Fig. 9 *Measured impedance at the PW when SW is open and short circuited*

in the open- and short-circuit modes, as shown in Fig. 9 in which the notations with arrows indicate the dominant parameters in the frequency range marked by the arrow [44–47].

In this paper, we used the HP4149 frequency response analyser with the frequency response range from 100 Hz–40 MHz.

The resistances R_p and R_s shown in Fig. 9 are the DC resistance components of SCTR. Therefore, as shown in Fig. 9, the resistances R_p and R_s can be obtained at low frequencies using a digital multimeter. The measured values of the resistances R_p and R_s are 0.05 and 0.025 Ω, respectively. The remaining parameters of Fig. 9, the magnetising inductance L_m and the leakage inductance

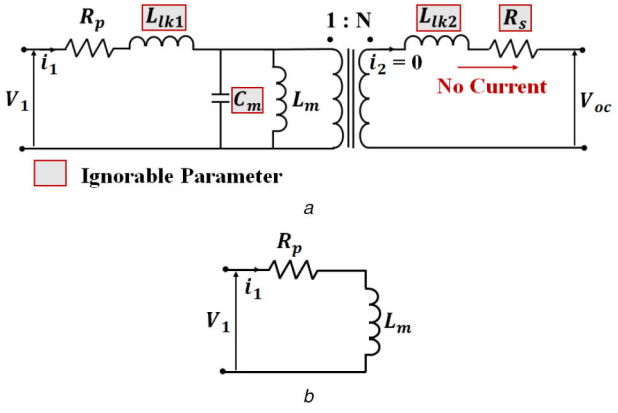

Fig. 10 *When the SW is open-circuited*
(a) MEC of SCTR, ***(b)*** Simplified MEC

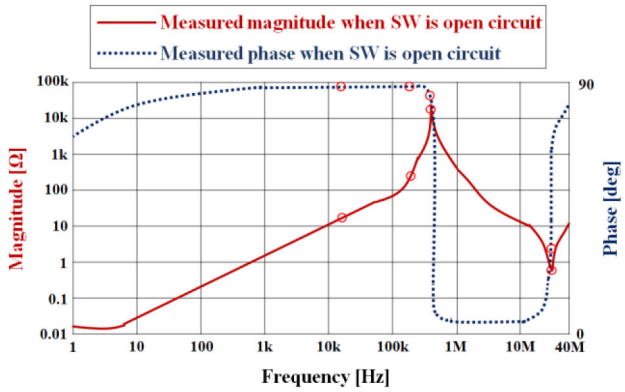

Fig. 11 *Measured value of primary impedance when the SW is open-circuited*

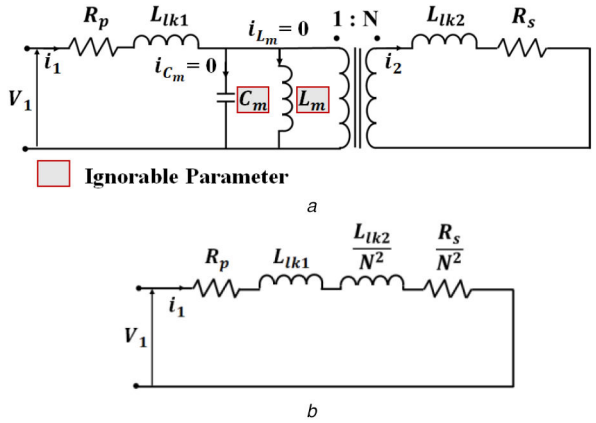

Fig. 12 *When the SW is short-circuited*
(a) MEC of SCTR, ***(b)*** Simplified MEC and the parameters of SW are reflected into the PW

L_{lk} are obtained through the SW open-circuit and short-circuit states, respectively, in Steps 3.2 and Step 3.3.

Since the inductance shows a non-linear characteristic depending on the frequency, it is necessary to limit the frequency range of interest based on the range of the resonance frequency and the phase of the impedance. The frequency range in which the phase of the PW impedance is decreasing is the interval in which the material characteristics and the temperature change with increasing frequency. Therefore, the range of the frequency should be limited to a phase close to 90 degrees. Otherwise, the capacitance is less non-linear with frequency variation.

3.3.2 Characteristic analysis of SCTR via the SW open-circuit test and MEC: As shown in Fig. 10*a*, L_{lk2} and R_S can be ignored because current does not flow in the SW part when the SW circuit is open. Moreover, the leakage inductance L_{lk1} and parasitic capacitance C_m can be neglected as well because they are only ~1% of the resistance R_p. Therefore, Fig. 10*a* can be simplified to Fig. 10*b* and (17) where the resistance R_p and the magnetising inductance L_m are unknown parameters.

The value of the resistance R_p in Step 3.1 measured by the PW open-circuit test, 0.05 Ω, can be applied in (17). As shown in Fig. 11, the inductance term is dominant between 100 Hz and the first resonance point at 624.30 Hz. Hence, 29.17 and 317.17 kHz are arbitrarily selected and their respective impedance values 387.96 and 26.81 Ω are substituted into (17) to obtain the inductance L_m of 195.05 µH.

$$|Z_{open}| = \sqrt{R_p^2 + (2\pi f L_m)^2} \tag{17}$$

By substituting the obtained values of the resonance frequency f_{r1} is 624.30 kHz and the magnetising inductance L_m is 195.05 µH into (18), the parasitic capacitance C_m between the windings can be calculated and its value is found to be 0.33 nF.

$$f_{r1} = \frac{1}{2\pi\sqrt{L_m C_m}} \tag{18}$$

The primary leakage inductance L_{lk1} is 0.11 µH can be obtained by substituting the value of the second resonance frequency f_{r2} of 25.48 MHz and the parasitic capacitance C_m calculated by (18) into (19).

$$f_{r2} = \frac{1}{2\pi\sqrt{L_{lk1} C_m}} \tag{19}$$

3.3.3 Characteristic analysis of SCTR via the SW short-circuit test and MEC: As illustrated in Fig. 12*a*, the parasitic capacitance C_m and magnetising inductance L_m can be ignored because their values are relatively larger than the values of the winding resistance R_p and leakage inductance L_{lk1}.

When the secondary-side parameters are reflected the primary side, Fig. 12*b* and (20) can be derived.

$$|Z_{short}| = \sqrt{\left(R_p + \frac{R_s}{N^2}\right)^2 + \left(2\pi f\left(L_{lk1} + \frac{L_{lk2}}{N^2}\right)\right)^2} \tag{20}$$

Among the parameters shown in Fig. 12*b* and (20), the resistance R_p, resistance R_s, and magnetising inductance L_{lk1} are obtained in the previous steps. Since the TR turns ratio is 2:1, N_2 can be 0.25. Finally, the unknown parameter of (20) is the leakage inductance L_{lk2}.

By randomly selecting two frequency points 360.83 kHz and 12.53 MHz in the inductance-dominated frequency range, which is between 100 kHz and the resonance frequency, and applying their respective impedance values of 303.85 mΩ and 9.12 Ω into (20), the leakage inductance L_{lk2} can be calculated as 0.025 µH (Fig. 13).

In this step, the MEC and its parameter values, which can effectively demonstrate the characteristics of SCTR, are proposed by using the experimental method and analytic method.

The parasitic capacitance values that are not normally included in the characteristic estimation are considered in this research to obtain more accurate values.

3.3.4 Final check of SCTR via data obtained from experiment and FEM: In this step, to verify the usefulness of the proposed analysis method, design method, and SCTR, the calculated values and experimental data are checked.

Specifically, the measured important characteristics of the SCTR, such as the magnetising inductance, leakage inductance, etc., are compared with the calculated data, design criteria, and design constraints. An example is shown in Table 6.

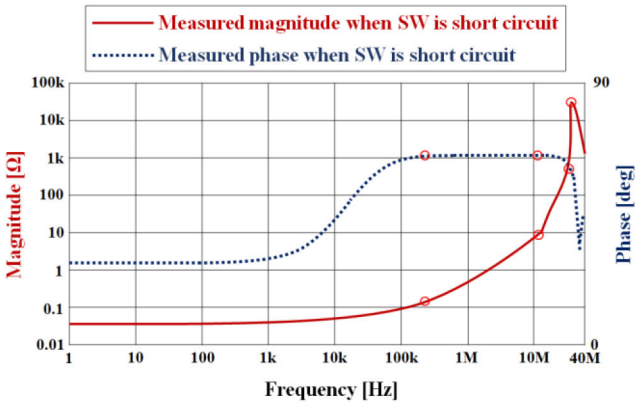

Fig. 13 *Measured value of primary impedance when the SW is short circuited*

Table 6 Comparison of parameter values of MEC obtained through FEM and experiment

Parameter	L_m	C_m	L_{lk1}	L_{lk2}
FEM results	197.06 μH	—	0.10 μH	0.023 μH
experimental results	195.0 5 μH	0.33 nF	0.11 μH	0.025 μH
error	1.01%	—	10.0%	8.7%

As tabulated in Table 6, the error of the magnetising inductance L_m between the calculated data, which was obtained via the proposed analysis method, and experimental data is ∼1%. However, the difference in the leakage inductance L_{lk1} between the calculated data and the experimental result is ∼10% because the skin and proximity effects were ignored in the calculations. The method for determining the value of inductance with non-linear characteristics according to frequency should be further discussed and researched. The above method only finds an approximate value. However, the overall errors are satisfactory, and it is confirmed that the proposed analysis method is correct.

In addition, the SCTR fabricated through the proposed analysis and design method meets the design requirements. Specifically, the magnetisation inductance is high with a high coupling coefficient of 0.9999. The leakage inductances are <0.01% of the magnetising inductance value. The efficiency is high at 98.65%.

From the above data at this step, it is checked whether the designed SCTR finally passes the design criteria within the design constraints. The usefulness of the proposed analysis method, design method, and SCTR are confirmed.

4 Conclusion

The industrial demands on PCS and TR have recently been focused on high efficiency and power density. However, it is difficult to achieve advancements in the efficiency and power density of PCS and TR by improving conventional technology. Hence, the significant implication of this paper is that innovative improvement of the efficiency and high power density of TR and PCS is possible by using the proposed novel and practical SCTR.

As the research on the characteristic analysis and design method of SCTR was insufficient, a useful and strategic analysis and design method, which covered the whole development process of SCTR, from design to experiment, was proposed in this paper.

The proposed analysis and design method can also be useful for studying analysis and design methods for numerous types of electrical machines.

Remarkably, the proposed SCTR can not only be commercialised and applied in TRs of different power levels but also can contribute to the advancement of related technologies and diverse types of electrical machines.

5 Acknowledgments

This study was supported by the Basic Science Research Program through the National Research Foundation of Korea funded by the Ministry of Education (2016R1D1A1B01008058) and by the Human Resources Development (20184030202070) of the Korea Institute of Energy Technology Evaluation and Planning (KETEP) grant funded by the Korea government Ministry of Trade, Industry, and Energy.

6 References

[1] Hsieh, Y.C., Chen, M.R., Cheng, H.L.: 'An interleaved flyback converter featured with zero-voltage transition', *IEEE Trans. Power Electron.*, 2011, **26**, (1), pp. 79–84

[2] Kohno, H., Molokov, S.: 'Finite element analysis of interfacial instability in aluminium reduction cells in a uniform, vertical magnetic field', *Int. J. Eng. Sci.*, 2007, **45**, (2–8), pp. 644–659

[3] Pareschi, F., Rovatti, R., Setti, G.: 'EMI reduction via spread spectrum in DC/DC converters: state of the art, optimization, and tradeoffs', *IEEE. Access.*, 2015, **3**, pp. 2857–2874

[4] Hurley, W.G., Wölfle, W.H., Breslin, J.G.: 'Optimized transformer design: inclusive of high-frequency effects', *IEEE Trans. Power Electron.*, 1998, **13**, (4), pp. 651–659

[5] Geng, C., Su, L., Wang, F.: 'Parameter identification and prediction of jiles–atherton model for DC-biased transformer using improved shuffled frog leaping algorithm and least square support vector machine', *IET Electr. Power Appl.*, 2015, **9**, pp. 660–669

[6] Lembeye, Y., Dang Bang, V., Lefèvre, G., *et al.*: 'Novel half-bridge inductive DC-DC isolated converters for fuel cell applications', *IEEE Trans. Energy Convers.*, 2009, **24**, (1), pp. 203–210

[7] Sippola, M., Sepponen, R.E.: 'Accurate prediction of high-frequency power-transformer losses and temperature rise', *IEEE Trans. Power Electron.*, 2002, **17**, (5), pp. 835–847

[8] Abdul Razak, A.R., Taib, S.: 'Design considerations of a high frequency power transformer'. Proc. Natl. Power Eng. Conf., Bangi, Malaysia, 2003, pp. 243–248

[9] Rashtchi, V., Rahimpour, E., Fotoohabadi, H.: 'Parameter identification of transformer detailed model based on chaos optimisation algorithm', *IET Electr. Power Appl.*, 2011, **5**, (2), p. 238

[10] Kheraluwala, M.H., Novotny, D.W., Divan, D.M.: 'Design considerations for high power high frequency transformers'. 21st Annual IEEE Conf. on Power Electronics Specialists, San Antonio, USA, 1990, pp. 734–742

[11] Chanane, A., Bouchhida, O., Houassine, H.: 'Investigation of the transformer winding high-frequency parameters identification using particle swarm optimisation method', *IET Electr. Power Appl.*, 2016, **10**, (9), pp. 923–931

[12] Saied, M.M., Hanafy, A.A., El-Gabaly, M.A., *et al.*: 'Optimal design parameters for A PV array coupled to a Dc motor via a Dc-Dc transformer', *IEEE Trans. Energy Convers.*, 1991, **6**, (4), pp. 593–598

[13] Kim Do-Hyun, P.J.-H.: 'High efficiency step-down flyback converter using coaxial cable coupled-inductor', *J. Power Electron.*, 2013, **13**, (2), pp. 214–222

[14] Rauls, M.S.: 'Design considerations for high-frequency coaxial winding power transformers', *IEEE Trans. Ind. Appl.*, 1993, **29**, (2), pp. 375–381

[15] Waltrich, G.: 'Inductances design of high-frequency coaxial transformers', *OALib*, 2016, **03**, (7), pp. 1–6

[16] Waltrich, G., Duarte, J.L., Hendrix, M.A.M.: 'Multiport converters for fast chargers of electrical vehicles - focus on high-frequency coaxial transformers'. 2010 Int. Power Electron. Conf. - ECCE Asia -, IPEC 2010, Sapporo, Japan, 2010, pp. 3151–3157

[17] Klontz, K.W., Divan, D.M., Novotny, D.W.: 'An actively cooled 120 kW coaxial winding transformer for fast charging electric vehicles', *IEEE Trans. Ind. Appl.*, 1995, **31**, (6), pp. 1257–1263

[18] Rauls, M.S., Novotny, D.W., Divan, D.M.: 'Design considerations for high frequency co-axial winding power transformers', *Conf. Rec. 1991 IEEE Ind. Appl. Soc. Annu. Meet.*, 1991, **29**, (2), pp. 946–952

[19] Taher, A., Sudhoff, S., Pekarek, S.: 'Calculation of a tape-wound transformer leakage inductance using the MEC model', *IEEE Trans. Energy Convers.*, 2015, **30**, (2), pp. 541–549

[20] Petkov, R.: 'Optimum design of a high-power, high-frequency transformer', *IEEE Trans. Power Electron.*, 1996, **11**, (1), pp. 33–42

[21] Hurley, W.G., Wilcox, D.J.: 'Calculation of leakage inductance in transformer windings', *IEEE Trans. Power Electron.*, 1994, **9**, (1), pp. 121–126

[22] Chang, L.: 'An improved fe inductance calculation for electrical machines', *IEEE Trans. Magn.*, 1996, **32**, (4 PART 2), pp. 3237–3245

[23] Ferreira, J.A.: 'Improved analytical modeling of conductive losses in magnetic components', *IEEE Trans. Power Electron.*, 1994, **9**, (1), pp. 127–131

[24] Ziger, I., Trkulja, B., Stih, Z.: 'Determination of core losses in open-core power voltage transformers', *IEEE. Access.*, 2018, **6**, pp. 29426–29435

[25] Urling, A.M., Niemela, V.A., Skutt, G.R., *et al.*: 'Characterizing high-frequency effects in transformer windings-a guide to several significant articles, fourth annu'. IEEE Appl. Power Electron. Conf. Expo., Baltimore, USA, 1989, pp. 373–385

[26] Shokrollahi, H., Janghorban, K.: 'Influence of additives on the magnetic properties, microstructure and densification of Mn-Zn soft ferrites', *Mater. Sci. Eng. B Solid-State Mater. Adv. Technol.*, 2007, **141**, (3), pp. 91–107

[27] Silveira, F.E.M., Kurcbart, S.M.: 'Inertial effects on good conductors: resistive heating and magnetic diffusion', *Int. J. Eng. Sci.*, 2012, **52**, pp. 22–29

[28] Lotfi, A.W., Wilkowski, M.A.: 'Issues and advances in high-frequency magnetics for switching power supplies', *Proc. IEEE*, 2001, **89**, (6), pp. 833–845

[29] Sullivan, C.R.: 'Optimal choice for number of strands in a litz-wire transformer winding', *IEEE Trans. Power Electron.*, 1999, **14**, (2), pp. 283–291
[30] Tsili, M.A., Amoiralis, E.I., Kladas, A.G., *et al.*: 'Optimal design of multi-winding transformer using combined FEM, taguchi and stochastic-deterministic approach', *IET Electr. Power Appl.*, 2012, **6**, (7), p. 437
[31] Colonel, W., McLyman, M.T.: '*Transformer and inductor design handbook*' (Kg Magnetics Inc., CA, USA, 2004, 3rd Edn.), pp. 44–60
[32] Chen, B., Li, L.: 'Semi-empirical model for precise analysis of copper losses in high-frequency transformers', *IEEE. Access.*, 2018, **6**, pp. 3655–3667
[33] Bagheri, M., Nezhivenko, S., Phung, B.T., *et al.*: 'Air core transformer winding disk deformation: a precise study on mutual inductance variation and its influence on frequency response spectrum', *IEEE. Access.*, 2017, **6**, (7476), pp. 7476–7488
[34] Tsili, M.A., Kladas, A.G., Georgilakis, P.S., *et al.*: 'Geometry optimization of magnetic shunts in power transformers based on a particular hybrid finite-element boundary-element model and sensitivity analysis', *IEEE Trans. Magn.*, 2005, **41**, (5), pp. 1776–1779
[35] Aboura, F., Touhami, O.: 'Effect of the GICs on magnetic saturation of asymmetric three-phase transformer', *IET Electr. Power Appl.*, 2017, **11**, (7), pp. 1306–1314
[36] Touhami, O., Aboura, F.: 'Integration of the hysteresis in models of asymmetric three-phase transformer: finite-element and dynamic electromagnetic models', *IET Electr. Power Appl.*, 2016, **10**, (7), pp. 614–622
[37] Cloud, M.J., Lebedev, L.P., Ponce-Vanegas, F.E.: 'Finite element method in equilibrium problems for a nonlinear shallow shell with an obstacle dedicated to prof. Leonid M. Zubov on the occasion of his 70th birthday', *Int. J. Eng. Sci.*, 2014, **80**, pp. 43–52
[38] Díaz-Chacón, J.M., Hernandez, C., Arjona, M.A.: 'Finite element and neural network approach for positioning a magnetic shunt on the tank wall of a transformer', *IET Electr. Power Appl.*, 2016, **10**, (9), pp. 827–833
[39] Chapman, S.J.: '*Electric machinery fundamentals*' (McGraw-Hill, NY, USA, 2013, 5thEdn.), vol. **3**, pp. 68–137
[40] Derbas, H.W., Williams, J.M., Koenig, A.C., *et al.*: 'A comparison of nodal-and mesh-based magnetic equivalent circuit models', *IEEE Trans. Energy Convers.*, 2009, **24**, (2), pp. 388–396
[41] Shilyashki, G., Pfützner, H.: 'Magnetic circuit modelling of transformer core induction – resolution and accuracy', *IET Electr. Power Appl.*, 2017, **11**, (7), pp. 1341–1346
[42] Mukherjee, P., Satish, L.: 'Construction of equivalent circuit of a transformer winding from driving-point impedance function – analytical approach', *IET Electr. Power Appl.*, 2012, **6**, (3), p. 172
[43] Xu, D.P., Lu, H.W., Jiang, Y.W., *et al.*: 'Analysis of sound pressure level of a balanced armature receiver considering coupling effects', *IEEE. Access.*, 2017, **5**, pp. 8930–8939
[44] Chaouche, M.S., Houassine, H., Moulahoum, S., *et al.*: 'BA to construction of equivalent circuit of a transformer winding from frequency response analysis measurement', *IET Electr. Power Appl.*, 2018, **12**, (5), pp. 728–736
[45] Ridley, R.: 'High frequency power transformer measurement and modeling', *Power Syst. Des. Eur.*, 2007, **14**, pp. 14–18
[46] Shintemirov, A., Tang, W.H., Wu, Q.H.: 'Transformer winding condition assessment using frequency response analysis and evidential reasoning', *IET Electr. Power Appl.*, 2010, **4**, (3), p. 198
[47] Hiraide, M., Nakajima, T., Koshizuka, T., *et al.*: 'Frequency response analysis for exact power transformer impedance', *CIRED - Open Access Proc. J.*, 2017, **2017**, (1), pp. 189–193